RESEARCH ARTICLE

Electrospun poly(lactic acid) nanofibers loaded with silver sulfadiazine/[Mg–Al]-layered double hydroxide as an antimicrobial wound dressing

João O. D. Malafatti[1,2] 🔘 | Marcela P. Bernardo[1] 🔘 | Francys K. V. Moreira[3] 🔘 |
Heloisa Ciol[4] 🔘 | Natalia M. Inada[4] 🔘 | Luiz H.C. Mattoso[1] 🔘 | Elaine C. Paris[1] 🔘

[1]National Nanotechnology Laboratory for Agriculture (LNNA), Embrapa Instrumentação, São Carlos, Brazil

[2]Department of Chemistry, Federal University of São Carlos, São Carlos, Brazil

[3]Department of Materials Engineering, Federal University of São Carlos, São Carlos, Brazil

[4]São Carlos Institute of Physics, University of São Paulo, São Carlos, Brazil

Correspondence
Elaine C. Paris, National Nanotechnology Laboratory for Agriculture (LNNA), Embrapa Instrumentação, 1452 XV de Novembro St, São Carlos 13560-970, Brazil.
Email: elaine.paris@embrapa.br

Poly(lactic acid) (PLA) is a versatile, bioabsorbable, and biodegradable polymer with excellent biocompatibility and ability to incorporate a great variety of active agents. Silver sulfadiazine (SDZ) is an antibiotic used to control bacterial infection in external wounds. Aiming to combine the properties of PLA and SDZ, hydrotalcite ([Mg–Al]-LDH) was used as a host matrix to obtain an antimicrobial system efficient in delivering SDZ from electrospun PLA scaffolds intended for wound skin healing. The structural reconstruction method was successfully applied to intercalate silver sulfadiazine in the [Mg–Al]-LDH, as evidenced by X-ray diffraction and thermogravimetric analyses. Observations by scanning electron microscopy revealed a good distribution of SDZ-[Mg–Al]-LDH within the PLA scaffold. Kinetics studies revealed a slow release of SDZ from the PLA scaffold due to the intercalation in the [Mg–Al]-LDH. *In vitro* antimicrobial tests indicated a significant inhibitory effect of SDZ-[Mg–Al]-LDH against *Escherichia* coli and *Staphylococcus* aureus. This antibacterial activity was sustained in the 2.5-wt% SDZ-[Mg–Al]-LDH–loaded PLA nanofibers, which also displayed excellent biocompatibility towards human cells. The multifunctionality of the PLA/SDZ-[Mg–Al]-LDH scaffold reported here is of great significance for various transdermal applications.

KEYWORDS

drug release, electrospinning, hydrotalcite, sulfadiazine silver, wound healing

1 | INTRODUCTION

Multifunctional wound dressings are urgently needed to accelerate wound healing processes, while simultaneously preventing microbial infections.[1,2] Traditional wound dressings are suitable when they keep a moist environment, provide thermal insulation, allow gases and fluid exchanges, are sterile and nonadherent to the wound, and can be easily removed without trauma.[3,4] Moreover, wound dressings become more attractive if they can provide an antimicrobial effect against external microorganisms.[5] This control prevents secondary infections and assists on the proper wound healing process.[6,7]

Wound dressings containing silver compounds are commonly used in clinical applications due to their effectiveness against several microorganisms. However, the release of the antimicrobial agent is often unsatisfactory,[8] leading to some shortcomings, including uncontrolled pharmacokinetics and deleterious side effects on nontarget tissues.[9] In this context, controlled or slow delivery systems are now highly considered for wound dressing applications because they could reduce side effects and allow localized release of precise antibiotic doses over an appropriate timescale.[10,11]

Layered double hydroxides (LDHs) are a class of inorganic solids able to control or delay the release of antimicrobial agents loaded in wound dressings. LDHs have attracted much attention for drug

delivery applications due to their intercalation properties, low toxicity, biocompatibility, high stability, pH-dependent solubility, and high cellular uptake behavior.[12] LDHs present the general stoichiometry $[M^{2+}_{1-x}M_x^{3+}(OH)_2]^{x+}(A^{n-})_{x/n} \cdot yH_2O$, where M^{2+} are bivalent cations, M^{3+} are trivalent cations, A^{n-} is a charge-balancing anion (CO_3^{2-}, NO_3^-, etc), and x is the molar ratio $[M^{3+}/(M^{3+} + M^{2+})]$ that ranges from 0.1 to 0.5. LDHs exhibit a $Mg(OH)_2$-like crystalline structure, in which a fraction of the M^{2+} cations at the octahedral sites is isomorphically replaced with M^{3+} cations.[13] The ensuing positive charge excess is counterbalanced by the A^{n-} species in the interlayer domains, which also contains H_2O molecules.[14] Owing to the so-called memory effect, large anionic species can be intercalated between the LDH layers. This effect consists in calcinating the LDH above 500°C to form a highly active mixed metal oxide, which is able to regenerate the original LDH structure by rehydration into a A^{n-}-rich aqueous solution under ambient conditions.[15]

Recently, the use of LDHs to control the release of drugs has opened up new applications of these layered solids in cosmetics and medicine.[16-19] However, there are still a few studies that elucidate the mechanism behind the release of these substances from LDHs. For instance, Joy et al[20] studied a [Zn–Al]-LDH as a host matrix for diclofenac sodium, whose release profile (90% of diclofenac sodium was released up to 240 h) was related to the intrinsic LDH properties. Dasgupta[21] intercalated ibuprofen (an anti-inflammatory drug) in a [Mg–Al]-LDH and observed that, after 15 hours, 50% of the drug was released to phosphate buffer solution. These reports point out the versatility of LDHs as host matrixes for controlled release of anionic drugs. On the other hand, LDHs are ineffective as wound dressings in their powder form, due to the poor adhesion of the particles to the injured skin surface.[22]

A promising approach to creating multifunctional wound dressings is the combination of the LDH release properties with electrospun biocompatible polymer nanofibers.[23,24] The electrospinning technique is capable of producing polymer scaffolds with large surface area and controlled porosity by tuning the processing conditions.[25] Electrospun scaffolds are also an alternative to control the release of hydrophilic and hydrophobic drugs.[26-28]

Electrospun nanofibers were effective in controlling the release of silver sulfadiazine (SDZ), a topical silver-based antibiotic clinically used for burn wound due to its broad inhibitory effect against multi–drug-resistant bacteria, while preserving its bactericidal activity.[8] Ullah et al[29] obtained zein nanofibers loaded with 0.6% SDZ, which showed antibacterial activity against _Bacillus sp_. and _Escherichia coli_. Also, electrospun polycaprolactone (PCL) nanofibers included with 1% SDZ were effective against _Staphylococcus aureus_ and _Staphylococcus epidermidis_ after 4 hours of contact.[30]

One of the leading polymers in the biomedical area is poly(lactic acid) (PLA), a green, bioabsorbable, and biodegradable polymer with excellent biocompatibility and ability to incorporate a great variety of active substances.[31-33] The degradation of PLA results in the formation of lactic acid, which is easily metabolized by the human body, being innocuous to the wound healing process.[34] Lee et al[30] obtained films based on PLA and poly(vinyl alcohol) (PVOH) incorporated with SDZ by spin-coating and casting method for treatment of burns in rat

cells. It was observed that the SDZ release last longer than 3 days, with low cytotoxicity and control over _S. aureus_ growth.

Systems based on polymers, LDHs, and anti-inflammatory drugs have been extensively disclosed in the literature,[22,23,35,36] but the use of SDZ-intercalated LDHs in electrospun polymer nanofibers aiming at antimicrobial wound dressing applications has not been published yet. Herein, we describe a suitable approach for the preparation of a new active wound dressing based on the electrospinning of PLA loaded with SDZ-intercalated [Mg–Al]-LDH. The PLA/SDZ-[Mg–Al]-LDH scaffolds were designed for (a) targeted release of SDZ in a slowed manner by its intercalation in [Mg–Al]-LDH, and (b) effective adherence of the SDZ-[Mg–Al]-LDH by using the biocompatible PLA nanofibers. The antimicrobial efficiency of the samples against pathogenic microorganisms was evaluated, and the SDZ release kinetics was assessed in phosphate buffer solution. The PLA/SDZ-[Mg–Al]-LDH scaffolds were also examined for their cytotoxicity on human dermal fibroblasts cells. The results were discussed with basis on microstructural and thermal characterizations.

2 | MATERIALS AND METHODS

2.1 | Materials

Silver(I) sulfadiazine ($C_{10}H_9AgN_4O_2S$, 98%, SDZ) were purchased from Sigma-Aldrich (St. Louis, Missouri). Commercial hydrotalcite (PURAL MG 61 HT) ($Mg_6Al_2(CO_3) \cdot (OH)_{16} \cdot 4H_2O$, [Mg–Al]-LDH) was kindly donated by Sasol Germany GmbH. Poly(lactic acid) (PLA) (M_M = 66 000 g mol^{-1}) was supplied by NatureWorks. Chloroform and dimethylsulfoxide (DMSO) were obtained from Synth (Brazil). All reagents were used as received. Decarbonated deionized water (ρ = 18.2 MΩ cm) obtained from Milli-Q system (Barnstead Nanopure Diamond, Thermo Fisher Scientific Inc, USA) was used in all experimental procedures.

2.2 | Intercalation of SDZ in [Mg–Al]-LDH

The intercalation of SDZ was performed using the structural reconstruction method, which is based on the "memory effect" of LDHs.[13] Briefly, the commercial [Mg–Al]-LDH was thermally treated at 600°C for 4 hours in a muffle furnace using a programmed heating rate of 30°C min^{-1}. Next, 500 mg of the calcined product were added to 250 mL of 0.1 g L^{-1} SDZ solution previously equilibrated at 25°C. The mixture was continuously agitated for 24 hours and then centrifuged at 11200 g for 10 minutes. The precipitate (SDZ-[Mg–Al]-LDH) was resuspended in water for storage in a freezer and further dried by lyophilization under vacuum of 1.33×10^{-4} bar (SuperModulyo freeze dryer, Thermo Fisher Scientific Inc, USA).

2.3 | Electrospinning of PLA incorporated with SDZ-[Mg–Al]-LDH

PLA scaffolds were obtained by the electrospinning technique. Initially, PLA was solubilized at 10% w/v in a mixture of chloroform and

DMSO (v/v = 3/1) under stirring at 25°C for 2 hours. Afterwards, 2.5% (w/w) of commercial [Mg–Al]-LDH and SDZ–[Mg–Al]-LDH were added to the PLA solution, and the stirring was prolonged for 1 hour. The electrospinning process was carried out at a voltage of 20 kV, using a solution feed rate of 0.8 mL h^{-1} and a needle tip to collector distance of 8 cm.[37] Pure PLA nanofibers and PLA nanofibers loaded with pure SDZ were prepared accordingly and used as controls. The concentration of SDZ in the PLA fibers was fixed at 0.25% (w/w).

2.4 | Characterizations

X-ray diffraction (XRD) measurements were performed using a Shimadzu XRD 6000 diffractometer with Ni-filtered Cu K$_\alpha$ radiation (λ = 1.5405 Å), in the 2θ range of 5° to 80°, with a scan speed of 1° per minute. Interplanar distances (d) were calculated using the classical Bragg equation (nλ = 2$d$senθ). Scanning electron microscopy (SEM) was conducted on JEOL microscope running at 15 kV. X-ray dispersive energy spectroscopy (EDS) was used to evaluate the dispersion of [Mg–Al]-LDH and SDZ within the PLA nanofibers. Attenuated total reflectance Fourier transform infrared (ATR-FTIR) spectroscopy was performed using a Bruker spectrometer with a spectral resolution of 2 cm^{-1}. Thermal degradation of samples was evaluated using a TGA Q500 thermo-analyzer (TA Instruments, USA). Samples (approximately 10 mg) were heated from 25°C to 850°C using a heating rate of 10°C min^{-1} under N$_2$ atmosphere (60 mL min^{-1}). Differential scanning calorimetry (DSC) was performed using a Q100 calorimeter (TA Instruments, USA) on samples (5-10 mg) placed in sealed aluminum crucibles and heated from 25°C to 200°C using heating rate of 10°C min^{-1} under N$_2$ atmosphere (50 mL min^{-1}).

2.5 | In vitro antimicrobial tests

The antimicrobial activity of SDZ and SDZ-[Mg–Al]-LDH was tested against *E. coli* (ATCC 11229) and *S. aureus* (ATCC 6538) by agar diffusion test, following the Kirby-Bauer method.[38] The strains of *E. coli* and *S. aureus* were cultivated in tubes containing Mueller Hinton liquid medium (Becton, Dickinson and Co, Sparks, Maryland) at 37°C for 24 hours to prepare bacterial suspensions with concentration of 10^6 CFU mL^{-1} adjusted by a 0.5 McFarland turbidity standard. Next, the SDZ and SDZ-[Mg–Al]-LDH samples were transferred to petri dishes containing Mueller Hinton solid medium previously inoculated with 10 μL of bacterial suspension. Controls without sample were also prepared for each strain. All petri dishes were incubated at 37°C for 24 hours, and the antimicrobial activity was evaluated by the formation of inhibitory zones. The experiments were conducted in triplicate.

2.6 | Kinetics of SDZ release in phosphate buffer

The release of equivalent doses of SDZ (5 mg L^{-1}) from all samples was studied in 20 mL of phosphate buffer solution (pH 7.4) under constant stirring at 25°C. The SDZ concentration was determined at selected time intervals by ultraviolet-visible (UV-vis) spectrophotometry on a Shimadzu UV-1601PC equipment, in the wavelength range between 200 and 400 nm. The experiments were conducted in triplicate.

2.7 | Cell culture and cytotoxicity assay by MTT

The cytotoxicity assay was conducted according to the ISO 0993-5:2009 protocol. Human dermal fibroblasts cells (HDFn) were cultivated at 37°C in humidified 5% CO$_2$ atmosphere in Dulbecco's modified Eagle medium (DMEM) supplemented with 10% fetal bovine serum (FBS) (v/v). For the cytotoxicity assay, cells were seeded at a density of 2 × 10^4 cells per well and stored in a heated chamber overnight before incubation with the scaffold extract. For the extract, scaffolds were sterilized with UVC radiation (λ = 254 nm) for 15 minutes each side followed by 24 and 168 hours of incubation in the red phenol-free cell culture medium DMEM supplemented with 5% FBS. The cell medium was replaced with the 24- or 168 hour-scaffold extract, and the cells were incubated in the heated chamber for at least 24 hours before the MTT assay. For the MTT assay, the scaffold-extract medium was replaced with red phenol–free DMEM containing MTT (5 μg/mL) and incubated for 4 hours and then replaced with 100 μL of DMSO before absorbance reading at λ = 570 nm in a microplate reader (Multiskan FC Microplate Photometer—ThermoFisher Scientific). Cell passages were between 4 and 8. All experiments were repeated in triplicate using five-well replicates for each time.

2.8 | Statistical analysis

Data were subjected to analysis of variance and multiple Duncan comparison test, assuming a confidence level of 95% (P < .05). Statistical analyses were performed using the software R version 3.6.0.

3 | RESULTS AND DISCUSSION

3.1 | Intercalation of SDZ in [Mg–Al]-LDH

LDHs exhibit the so-called memory effect, which has allowed them to be intercalated with different anionic molecules. The reconstruction method was first carried out using pure water to examine the memory effect in the commercial [Mg–Al]-LDH. Figure 1A presents the XRD patterns of the commercial [Mg–Al]-LDH, the calcinated product, and the corresponding sample obtained after 24 hours of immersion in water. The XRD pattern of [Mg–Al]-LDH (Figure 1A[1]) denotes the hexagonal lattice with rhombohedral 3R symmetry typical of LDHs. The basal spacing calculated from the (003) reflection (d_{003}-spacing) by the Bragg law was 0.76 nm, in accordance with previous values reported for hydrotalcite like-LDHs.[39,40] After thermal treatment, the
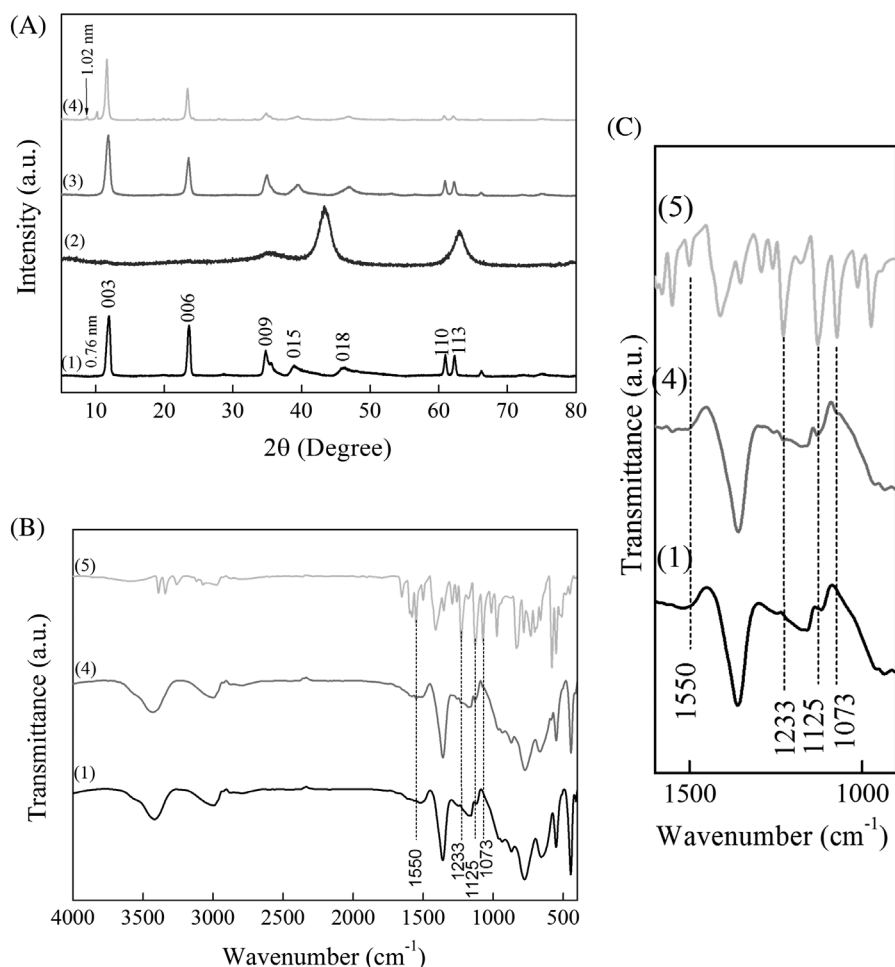
FIGURE 1 (A) XRD patterns, (B) ATR-FTIR spectra, (C) ATR-FTIR spectra in the region 1550-1000 cm^{-1} of (1) commercial [Mg–Al]-LDH; (2) calcined [Mg–Al]-LDH; (3) [Mg–Al]-LDH reconstructed in water; (4) [Mg–Al]-LDH reconstructed in 0.1 g L^{-1} SDZ solution and (5) pure SDZ

XRD pattern in (Figure 1A[2]) displays reflections indexed to the MgO phase (*Fm3̄cm*, JCPDS 45-0946), indicating the total collapse of the LDH structure after calcination.[13] After immersion in water, the layered structure is restored, as observed by the presence of the typical LDH reflections in the XRD pattern in Figure 1A(3).

Figure 1A(4) shows the XRD pattern of [Mg–Al]-LDH reconstructed in 0.1 mg L^{-1} SDZ solution (SDZ-[Mg–Al]-LDH). It can be observed the characteristic reflections of LDHs, indicating that the [Mg–Al]-LDH structure was restored even in the presence of SDZ. In addition, two new reflections were identified at 10.2° and 8.7° of 2θ. SDZ is a crystalline antimicrobial compound that exhibits a reflection at 2θ = 10.20°.[41] On the other hand, the reflection at 2θ = 8.7° may relate to an increase of the d_{003}-spacing to 1.02 nm, suggesting the intercalation of SDZ between the [Mg–Al]-LDH lamellas.

The intercalation of SDZ in the [Mg–Al]-LDH was also examined by FTIR spectroscopy. Figure 1B(1) shows the ATR-FTIR spectrum of the commercial [Mg–Al]-LDH. An intense band around 3420 cm^{-1} is observed, attributed to stretching vibration of hydroxyl groups of the metal hydroxide layers and interlayer water molecules.[42] The band at approximately 1350 cm^{-1} indicates the stretching vibration of interlayer CO_3^{2-} anions, as expected.[43] A further vibration related to metal-oxygen bond stretching was observed at 700 cm^{-1}. The ATR-FTIR spectrum of pure SDZ (Figure 1B[5]) displayed bands at around

1550 cm^{-1}, which are ascribed to stretching of phenyl structures conjugated to NH_2 groups, and a vibration band at 1233 cm^{-1}, which is attributed to the asymmetric stretching of S=O bonds. Also, the vibration bands at 3344 and 3394 cm^{-1} are ascribed to stretching vibration modes of NH_2 group.[44] The presence of SDZ in the [Mg–Al]-LDH structure was indicated by the ATR-FTIR spectrum in Figure 1B(4), particularly by the SDZ vibration bands at 1233, 1125, and 581 cm^{-1} that overlapped with the [Mg–Al]-LDH bands. The interaction between SDZ and [Mg–Al]-LDH is based on electrostatic attraction between the negatively charged N of the SDZ aromatic ring and the positively charged Al^{3+} sites in the [Mg–Al]-LDH layers, hydrogen bonding,[45] in addition to ligand exchange and ion exchange mechanisms.[46] Therefore, according to the XRD and FTIR results, SDZ was intercalated within the [Mg–Al]-LDH galleries. Adsorption of SDZ molecules on the external [Mg–Al]-LDH particle surface may have also occurred as well.

The thermal stability of the [Mg–Al]-LDH intercalated with SDZ was assessed by TG/DTG (Figure 2). The commercial [Mg–Al]-LDH exhibited mass loss events occurring in three main temperature ranges (Figure 2A). The first mass loss (165°C) is ascribed to the elimination of adsorbed water molecules. The mass loss at around 215°C relates to elimination of interlayer water molecules, whereas the mass loss above 300°C corresponds to the dihydroxylation of the
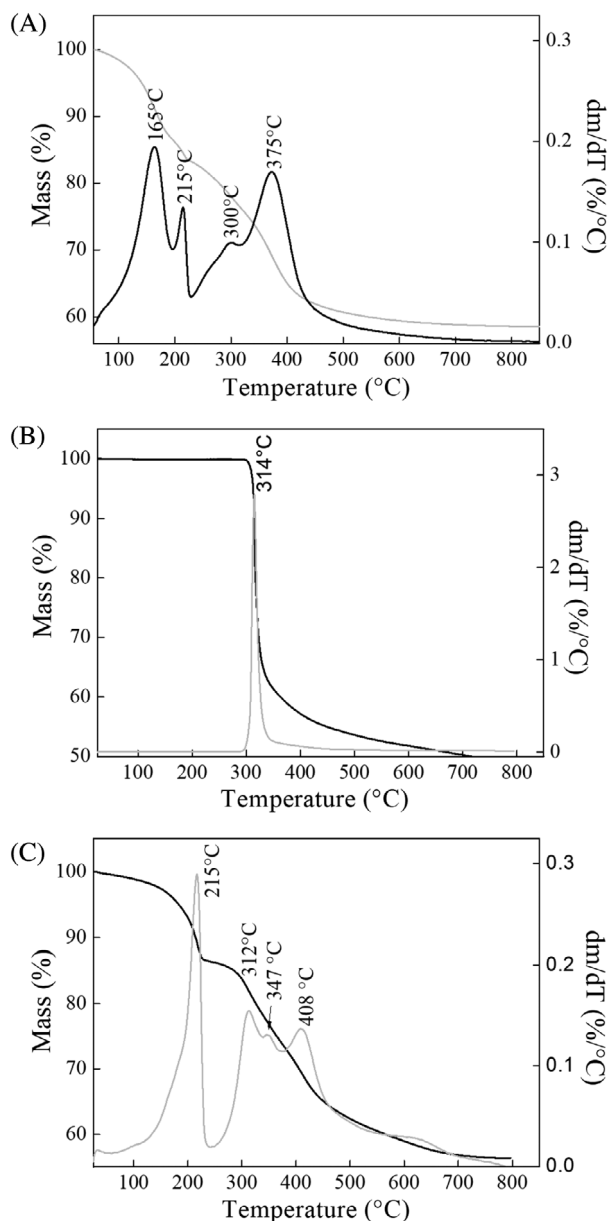
FIGURE 2 TG and DTG curves of (A) commercial [Mg–Al]-LDH, (B) pure SDZ, (C) SDZ-[Mg–Al]-LDH

hydrotalcite layers. The decomposition of the CO_3^{2-} anions occurs at higher temperatures, while [Mg-Al]-LDH is converted into mixed metal oxides, such as MgO and Al_2O_3, which remain as final degradation products,[47-49] as evidenced by XRD (Figure 1A[2]). Yet pure SDZ presents a major mass loss at approximately 314°C (Figure 2B).[50] The TG/DTG curves of SDZ-[Mg-Al]-LDH indicate two manners of interaction between SDZ and [Mg-Al]-LDH due to the presence of two mass losses at around 312°C and 347°C (Figure 2C). The fraction of SDZ molecules effectively intercalated between the [Mg-Al]-LDH layers probably had its thermal stability increased; therefore, the mass loss at 347°C corresponds to this SDZ fraction. The SDZ molecules physically adsorbed on the external [Mg-Al]-LDH surface represent no changes in the thermal stability of SDZ, as observed by the mass loss at 312°C.[22,46] In addition, SDZ molecules may be replacing water molecules in the [Mg-Al]-LDH galleries. Therefore, the mass loss at

165°C to 220°C related to the interlayer water is significantly reduced in Figure 2C. The DTG peak at around 408°C may be related to the decomposition of the counter anions and oxide formation.[51] With basis on these results, the loading capacity of SDZ in the [Mg-Al]-LDH was calculated to be 0.005 mg L^{-1}.

Disc diffusion tests were conducted using *E. coli* and *S. aureus* to assess the antimicrobial activity of SDZ against gram-negative and gram-positive bacteria, respectively, after intercalation in the [Mg-Al]-LDH (Figure S1). According to the inhibitory zone diameters reported in Table 1, SDZ displayed antimicrobial activity against both bacteria, but its inhibitory effect was more pronounced on *S. aureus*, which is the second most common bacterium found in burn injuries.[52] The antimicrobial activity of SDZ is due to the presence of both Ag^+ and sulfadiazine ions, which act in synergism, mainly on the base pairs of the DNA helix structure, inhibiting the microbial cell transcription process.[53-55]

It can be further observed from Figure S1 that SDZ-[Mg–Al]-LDH exhibited similar antimicrobial activity as pure SDZ, forming visible inhibitory zones against both bacteria. This means that [Mg–Al]-LDH exhibited the capacity of releasing SDZ, confirming that the intercalation can be reverted, if the external conditions are favorable.[56] These results suggest that [Mg–Al]-LDH acted as a carrier matrix for SDZ, with the advantage of increasing the chemical stability of this antimicrobial agent. The SDZ-[Mg–Al]-LDH was then incorporated in the PLA nanofibers by electrospinning to develop antimicrobial scaffolds for wound healing, especially for burned skin injuries.

3.2 | Characterization of electrospun PLA scaffolds loaded with SDZ-[Mg–Al]-LDH

SEM was performed to elucidate the shape and diameters of the electrospun PLA nanofibers. SEM micrographs of the pure PLA, PLA-SDZ, PLA-[Mg–Al]-LDH, and PLA-SDZ-[Mg–Al]-LDH scaffolds are shown in Figure 3. The nanofibers incorporated with 2.5% (w/w)

TABLE 1 Inhibitory zone diameters for *E. coli* and *S. aureus* determined by disc diffusion tests

Sample	*E. coli*, mm	*S. aureus*, mm
Pure SDZ	2.60 ± 0.26	4.87 ± 0.12
SDZ-[Mg–Al]-LDH	2.13 ± 0.45	4.28 ± 0.13

[Mg–Al]-LDH and 0.25% (w/w) SDZ exhibited higher average diameter than that of the pure PLA nanofibers. This is probably due to the good distribution of these fillers within the PLA nanofibers, as reported by several authors.[57-59] Figure 3E displays the SEM micrographs and EDS elemental mapping of the PLA/SDZ-[Mg–Al]-LDH scaffold, in which the dispersion level of the [Mg–Al]-LDH particles is suggested by the Mg and Al signals. The micrographs suggest that the SDZ-[Mg–Al]-LDH particles did not form large agglomerates within the PLA nanofibers, meaning their proper distribution throughout the scaffold. This is a positive result because the scaffold can promote antimicrobial inhibition regardless of the side placed in contact with the wound.[60]

The electrospun scaffolds were also studied by FTIR spectroscopy (Figure S2). The ATR-FTIR spectrum of the pure PLA scaffold displayed the typical vibrational bands of PLA, including the band at around 1755 cm^{-1} due to stretching vibration of C=O bonds, and at approximately 1045 cm^{-1}, which corresponds to the υC–CH$_3$ stretching.[61] The presence of the SDZ-[Mg–Al]-LDH in the scaffold was evidenced by the LDH vibration band at 500 cm^{-1}.

Figure 4A presents the XRD patterns of the electrospun PLA–based scaffolds. The XRD pattern of the pure PLA sample showed a wide band between 10° and 40° of 2θ, which suggests the amorphous state of PLA in the electrospun nanofibers.[23] Although the crystalline nature of SDZ, no reflections ascribed to the antimicrobial drug were observed in the XRD pattern of the PLA/SDZ scaffold. Similarly, the XRD pattern of the PLA/[Mg–Al]-LDH scaffold displayed no
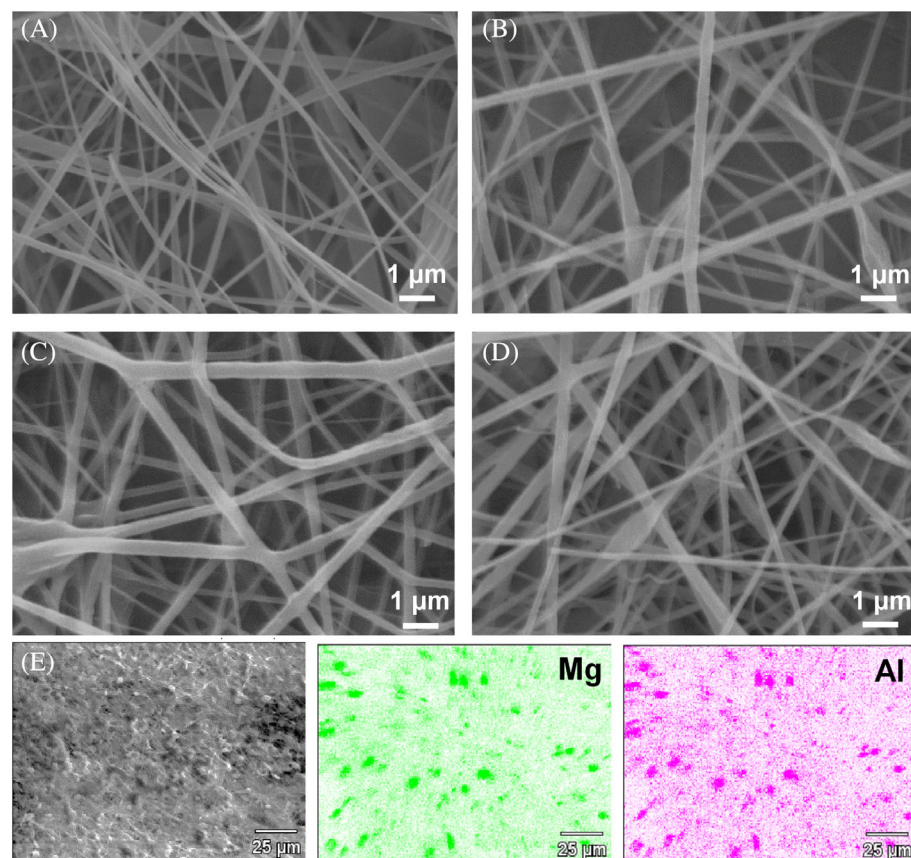
FIGURE 3 Scanning electron microscopy (SEM) micrographs of the electrospun scaffolds (A) pure PLA, (B) PLA/SDZ, (C) PLA/[Mg–Al]-LDH, and (D) PLA/SDZ-[Mg–Al]-LDH, (E) EDS-SEM elemental mapping of PLA-SDZ-[Mg–Al]-LDH nanofibers [Color figure can be viewed at wileyonlinelibrary.com]

TABLE 2 Summary of DSC results for the PLA-based electrospun scaffolds

Sample	T_g, °C	T_c, °C	T_m, °C	ΔH_m, J/g
PLA	59.4	85.2	170.0	42.1
PLA-SDZ	59.3	76.2	169.5	41.1
PLA-LDH	55.9	79.2	166.7	47.1
PLA-SDZ-[Mg–Al]-LDH	59.7	81.1	167.7	47.7

characteristic reflections of [Mg–Al]-LDH.[22] Both results may be explained by the low concentrations of SDZ and [Mg–Al]-LDH incorporated in the PLA nanofibers, whose structure remained essentially amorphous, regardless of the presence of both components.

Figure 4B shows the DSC curves of the PLA scaffolds incorporated with [Mg–Al]-LDH, SDZ, and SDZ-[Mg–Al]-LDH. All samples were amorphous at room temperature as indicated by the XRD results and exhibited the typical PLA cold-crystallization at 85°C. The glass transition temperature (T_g), melting temperature (T_m), crystallization temperature (T_c), and enthalpy (ΔH) data are summarized in Table 2.

The typical thermal events of PLA were found for the pure scaffold, with T_g at 59°C, T_c at 85°C, and T_m at 170°C. After the addition of [Mg–Al]-LDH and SDZ, no changes were observed in these thermal parameters, confirming that the incorporation of the [Mg–Al]-LDH and SDZ did not alter the morphology of the PLA chains in the electrospun nanofibers. The amorphous structure of the PLA matrix favors the release of SDZ through diffusion mechanisms, possibly implying in an effective antimicrobial activity of the PLA-SDZ-[Mg–Al]-LDH scaffolds.

The success of electrospun antimicrobial scaffolds to act as wound dressings relies, among other aspects, on their ability to control, or at least slow up, the release of the antimicrobial agent. To evaluate the SDZ release from the electrospun PLA nanofibers, a kinetic study was performed in phosphate buffer solution, as represented in Figure 5A. SDZ displays slow solubility in this medium; thus, its concentration increased gradually over time, as also observed in earlier reports[55] (Figure 5A[1]).

Considering the SDZ-[Mg–Al]-LDH sample (Figure 5A[2]), the amount of SDZ released after 4 hours may be attributed to the SDZ molecule fraction adsorbed on the external [Mg–Al]-LDH particle surface.[46] This result was probably due to the ion exchange between the PO_4^{3-} anions present in the buffer medium and the SDZ molecules.[62] However, it can be observed that the amount of SDZ released from SDZ-[Mg–Al]-LDH was lower than that from pure SDZ, revealing that the intercalation delayed the SDZ release kinetics.

The SDZ release profile from the PLA/SDZ scaffold (Figure 5A[3]) was similar to that of pure SDZ, suggesting a little influence of the PLA matrix in the SDZ release process. This result may be due to a low affinity between SDZ and PLA.[63] The lower SDZ concentration values observed are due the lower amount of SDZ in the PLA scaffold in relation to the pure drug. The PLA/SDZ-[Mg–Al]-LDH scaffold (Figure 5A[4]) showed an SDZ release profile quite similar to that of SDZ-[Mg–Al]-LDH until 4 hours. In other words, the amount of SDZ
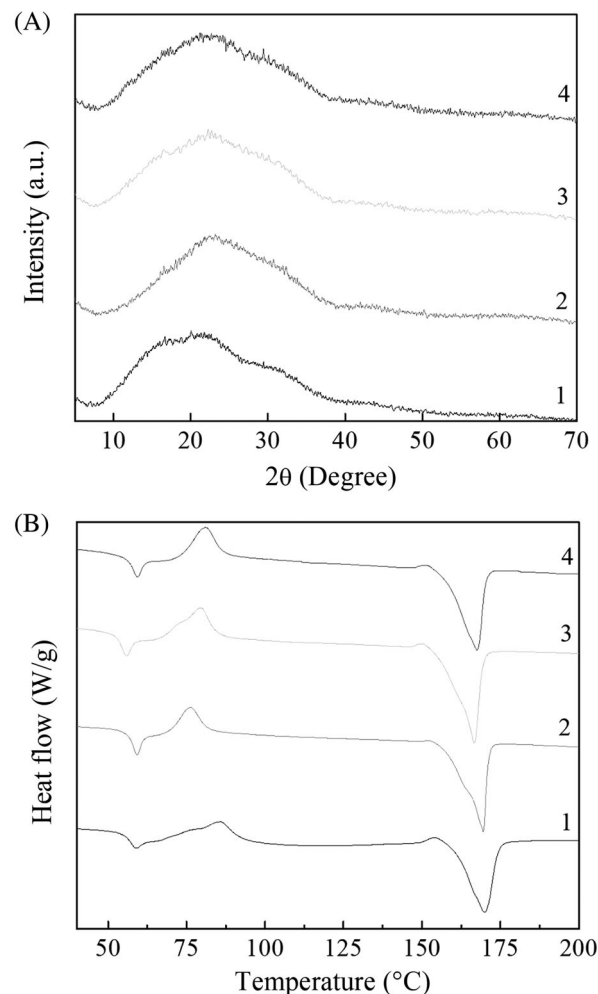
FIGURE 4 (A) XRD patterns of (1) pure PLA, (2) PLA/SDZ, (3) PLA/[Mg–Al]-LDH, and (4) PLA-SDZ-[Mg–Al]-LDH scaffolds obtained by electrospinning. (B) Differential scanning calorimetry (DSC) curves of (1) pure PLA, (2) PLA/SDZ, (3) PLA-/[Mg–Al]-LDH, and (4) PLA/SDZ-[Mg–Al]-LDH scaffolds obtained by electrospinning

released accounts for the SDZ molecule fraction dispersed within the PLA matrix. However, after 4 hours, the amount of SDZ released was expressively lower in comparison with pure SDZ, but the release was sustained for a longer period. Considering the application of PLA/SDZ-[Mg–Al]-LDH scaffold as a wound dressing, such a release profile is very advantageous, because the antimicrobial agent is released over a long period, avoiding the necessity of extra doses of SDZ and dressing renewal.[4]

The SDZ release mechanism from the PLA/SDZ-[Mg–Al]-LDH scaffold is schematically proposed in Figure 5B. Initially, the scaffold allows the release of the SDZ molecules dispersed throughout the amorphous PLA matrix by diffusion (Figure 5B[a]). In the second step, the SDZ-[Mg–Al]-LDH is released from the nanofibers, enabling the release of the SDZ molecules intercalated in the LDH galleries by ion exchange (Figure 5B[b]). According to this mechanism, the [Mg–Al]-LDH served to delay the SDZ release kinetics, creating a second drug dose application effect. It is worth pointing
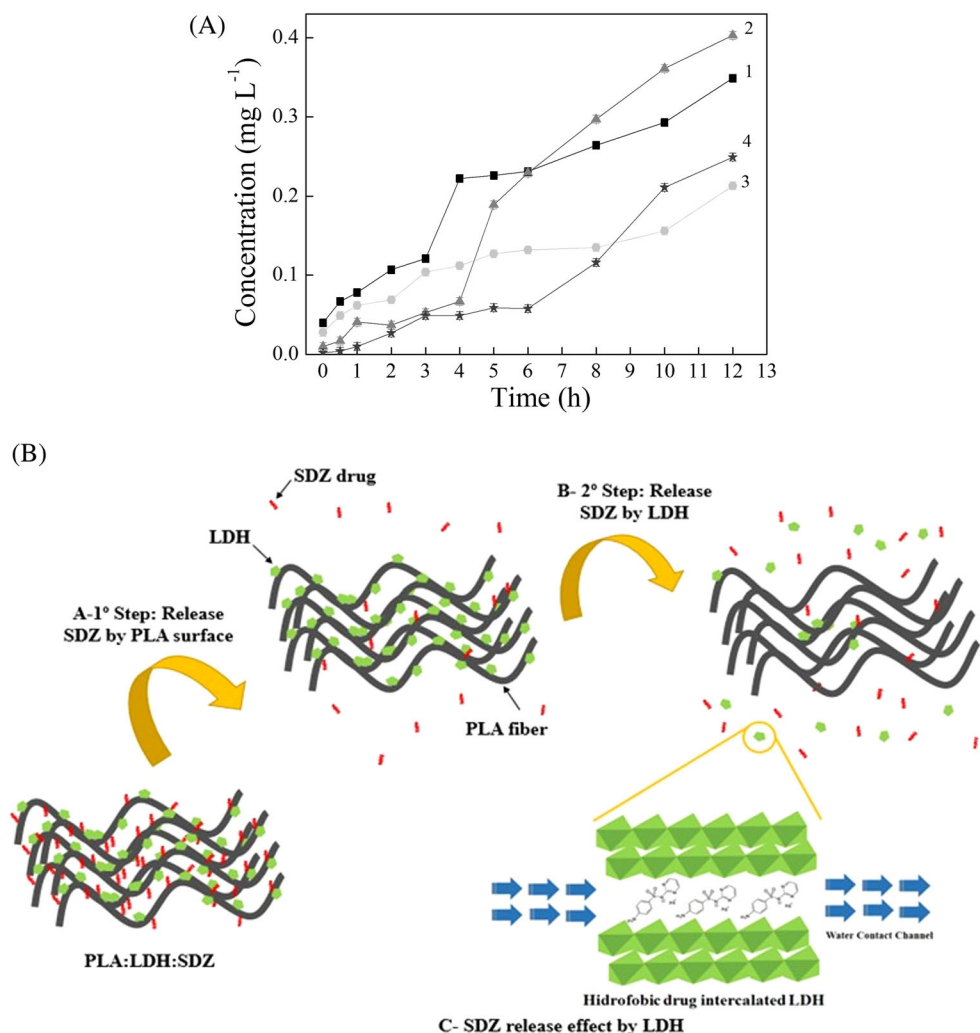
(A)

(B)

out that [Mg–Al]-LDH might have facilitated the SDZ solubilization by increasing the contact between the drug and aqueous medium (Figure 5B[c]). Thus, the PLA/SDZ-[Mg–Al]-LDH scaffold provides an alternative modulation for dressing and transdermal delivery of SDZ, sustaining the antimicrobial drug availability for an extended period.

3.3 | In vitro study of cell viability

MTT assays were performed to study the cytotoxicity of the SDZ-functionalized PLA/SDZ-[Mg–Al]-LDH scaffold (Figure 6). Silver, either as ions or nanoparticles, is a big concern to be given much attention due to its potential cytotoxicity.[64] Liu et al demonstrate that free silver sulfadiazine has significant reduction effect on the cell viability.[65] Figure 6 reveals that the PLA/SDZ-[Mg–Al]-LDH scaffold presented great cell biocompatibility after 24 and 168 hours, with cell viability of 97% and 98%, respectively. Therefore, the incorporation of the SDZ-[Mg–Al]-LDH in the PLA nanofibers promoted, at the same time, enough release of SDZ for effective antimicrobial effect and no significant effect on human cell viability. In other words, the
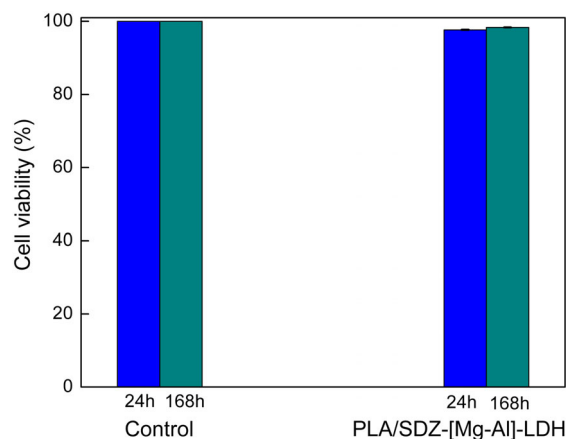
FIGURE 6 Results of indirect cytotoxicity of PLA/SDZ-[Mg–Al]-LDH scaffold on HDFn cells after 24 and 168 hours [Color figure can be viewed at wileyonlinelibrary.com]

membrane exhibited excellent biocompatibility, which is vital in the fine tuning of the delivery system intended for wound dressing applications.

4 | CONCLUSIONS

The electrospinning technique was successfully applied in the production of PLA scaffolds loaded with SDZ-intercalated [Mg–Al]-LDH. The [Mg–Al]-LDH was effective against *E. coli* and *S. aureus* when loaded with SDZ, and it was also an efficient carrier matrix that slowed the release rate of SDZ from the PLA scaffolds. In addition, the functionalized scaffolds exhibited suitable in vitro compatibility on fibroblast cells. The functionalities of the electrospun PLA/LDH-SDZ scaffolds reported here are key for antimicrobial wound dressings, leading to new strategies towards the development of controlled release systems for poorly water-soluble drugs, such as SDZ, opening up a broader range of transdermal membrane applications.

ORCID

João O. D. Malafatti https://orcid.org/0000-0002-7551-0510
Marcela P. Bernardo https://orcid.org/0000-0001-7788-8034
Francys K. V. Moreira https://orcid.org/0000-0001-6368-3177
Heloisa Ciol https://orcid.org/0000-0002-7539-023X
Natalia M. Inada https://orcid.org/0000-0003-1940-186X
Luiz H.C. Mattoso https://orcid.org/0000-0001-7586-1014
Elaine C. Paris https://orcid.org/0000-0001-8599-9674

REFERENCES

1. Wang J, Planz V, Vukosavljevic B, Windbergs M. Multifunctional electrospun nano fibers for wound application—novel insights into the control of drug release and antimicrobial activity. *Eur J Pharm Biopharm*. 2018;129(May):175-183. https://doi.org/10.1016/j.ejpb.2018.05.035.
2. Goh YF, Shakir I, Hussain R. Electrospun fibers for tissue engineering, drug delivery, and wound dressing. *J Mater Sci*. 2013;48(8):3027-3054. https://doi.org/10.1007/s10853-013-7145-8.
3. Vowden K, Vowden P. Wound dressings: principles and practice. *Surg (United Kingdom)*. 2017;35(9):489-494. https://doi.org/10.1016/j.mpsur.2017.06.005.
4. Zahedi P, Rezaeian I, Ranaei-Siadat SO, Jafari SH, Supaphol P. A review on wound dressings with an emphasis on electrospun nanofibrous polymeric bandages. *Polym Adv Technol*. 2010;21(2):77-95. https://doi.org/10.1002/pat.1625.
5. Rodríguez-Tobías H, Morales G, Ledezma A, Romero J, Grande D. Novel antibacterial electrospun mats based on poly(D,L-lactide) nanofibers and zinc oxide nanoparticles. *J Mater Sci*. 2014;49(24): 8373-8385. https://doi.org/10.1007/s10853-014-8547-y.
6. Luan J, Wu J, Zheng Y, et al. Impregnation of silver sulfadiazine into bacterial cellulose for antimicrobial and biocompatible wound dressing. *Biomed Mater*. 2012;7(6):065006. https://doi.org/10.1088/1748-6041/7/6/065006.
7. Becaro AA, Puti FC, Correa DS, Paris EC, Marconcini JM, Ferreira MD. Polyethylene films containing silver nanoparticles for applications in food packaging: characterization of physico-chemical and anti-microbial properties. *J Nanosci Nanotechnol*. 2014;15(3): 2148-2156. https://doi.org/10.1166/jnn.2015.9721.
8. Ito K, Saito A, Fujie T, et al. Sustainable antimicrobial effect of silver sulfadiazine-loaded nanosheets on infection in a mouse model of partial-thickness burn injury. *Acta Biomater*. 2015;24:87-95. https://doi.org/10.1016/j.actbio.2015.05.035.
9. Xiang Y, Liu X, Mao C, et al. Infection-prevention on Ti implants by controlled drug release from folic acid/ZnO quantum dots sealed titania nanotubes. *Mater Sci Eng C*. 2018;85(January):214–224. doi: 10.1016/j.msec.2017.12.034.
10. Ning LG, Kang E, Wang YB, Hu XF, Xu LQ. Recent developments in controlled release of antibiotics. *Curr Pharm des*. 2018;24:911-925. https://doi.org/10.2174/1381612824666180315094947.
11. Akduman C, Özgüney I, Kumbasar EPA. Preparation and characterization of naproxen-loaded electrospun thermoplastic polyurethane nanofibers as a drug delivery system. *Mater Sci Eng C*. 2016;64:383-390. https://doi.org/10.1016/j.msec.2016.04.005.
12. Ribeiro LNM, Alcântara ACS, Darder M, Aranda P, Araújo-moreira FM, Ruiz-hitzky E. Pectin-coated chitosan–LDH bionanocomposite beads as potential systems for colon-targeted drug delivery. *Int J Pharm*. 2014;463(1):1-9. https://doi.org/10.1016/j.ijpharm.2013.12.035.
13. Bernardo MP, Moreira FKV, Colnago LA, Ribeiro C. Physico-chemical assessment of [Mg-Al-PO$_4$]-LDHs obtained by structural reconstruction in high concentration of phosphate. *Colloids Surfaces A Physicochem Eng Asp*. 2016;497:53-62. https://doi.org/10.1016/j.colsurfa.2016.02.021.
14. Radha AV, Kamath PV, Shivakumara C. Mechanism of the anion exchange reactions of the layered double hydroxides (LDHs) of Ca and Mg with Al. *Solid State Sci*. 2005;7:1180-1187. https://doi.org/10.1016/j.solidstatesciences.2005.05.004.
15. Yu Q, Zheng YY, Wang Y, et al. Adsorptive removal of phosphate by Mg–Al and Zn–Al layered double hydroxides: kinetics, isotherms and mechanisms. *J Hazard Mater*. 2010;124(1–3):36-42. https://doi.org/10.1016/j.jhazmat.2009.12.063.
16. Komarala EP, Doshi S, Thiyagarajan S, Aslam M, Bahadur D. Studies on drug release kinetics and antibacterial activity against drug-resistant bacteria of cefotaxime sodium loaded layered double hydroxide–fenugreek nanohybrid. *RSC Adv*. 2018;42:129-136. https://doi.org/10.1039/c7nj03622a.
17. Ballarin B, Mignani A, Mogavero F, Gabbanini S, Morigi M. Hybrid material based on ZnAl hydrotalcite and silver nanoparticles for deodorant formulation. *Appl Clay Sci*. 2015;114:303-308. https://doi.org/10.1016/j.clay.2015.06.014.
18. Foroutan SM, Ettehadi H, Formulation THR. In vitro evaluation of silver sulfadiazine spray. *Iran J Pharm Res*. 2002;1(April):47-49.
19. Tang L, Cheng H, Cui S, et al. DL-mandelic acid intercalated Zn–Al layered double hydroxide: a novel antimicrobial layered material. *Colloids Surfaces B Biointerfaces*. 2018;165:111-117. https://doi.org/10.1016/j.colsurfb.2018.02.017.
20. Joy M, Iyengar SJ, Chakraborty J, Ghosh S. Layered double hydroxide using hydrothermal treatment: morphology evolution , intercalation and release kinetics of diclofenac sodium. *Front Mater Sci*. 2017;11(4): 395-408.
21. Dasgupta S. Controlled release of ibuprofen using Mg Al LDH nano carrier. *IOP Conf Ser Mater Sci Eng*. 2017;225:012005. https://doi.org/10.1088/1757-899X/225/1/012005.
22. Miao YE, Zhu H, Chen D, Wang R, Tjiu WW, Liu T. Electrospun fibers of layered double hydroxide/biopolymer nanocomposites as effective drug delivery systems. *Mater Chem Phys*. 2012;134(2–3):623-630. https://doi.org/10.1016/j.matchemphys.2012.03.041.
23. Zhao N, Shi S, Lu G, Wei M. Polylactide (PLA)/layered double hydroxides composite fibers by electrospinning method. *J Phys Chem Solid*. 2008;69(5–6):1564-1568. https://doi.org/10.1016/j.jpcs.2007.10.046.
24. Valarezo E, Tammaro L, González S, Malagón O, Vittoria V. Fabrication and sustained release properties of poly(ε-caprolactone) electrospun fibers loaded with layered double hydroxide nanoparticles intercalated with amoxicillin. *Appl Clay Sci*. 2013;72:104-109. https://doi.org/10.1016/j.clay.2012.12.006.

25. Anton Formhals. Production of artificial fibers. 1937:1936–1938.

26. Lu P, Ding B. Applications of electrospun fibers. *Recent Pat Nanotechnol*. 2008;2(3):169-182. https://doi.org/10.2174/187221008786369688.

27. Jalvandi J, White M, Truong YB, Gao Y, Padhye R, Kyratzis IL. Release and antimicrobial activity of levofloxacin from composite mats of poly (ε-caprolactone) and mesoporous silica nanoparticles fabricated by core-shell electrospinning. *J Mater Sci*. 2015;50(24):7967-7974. https://doi.org/10.1007/s10853-015-9361-x.

28. Hivechi A, Bahrami SH, Siegel RA. Drug release and biodegradability of electrospun cellulose nanocrystal reinforced polycaprolactone. *Mater Sci Eng C*. 2019;94(September 2018):929-937. https://doi.org/10.1016/j.msec.2018.10.037.

29. Ullah S, Hashmi M, Khan MQ, Kharaghani D. Silver sulfadiazine loaded zein nanofiber mats as a novel wound dressing. *RSC Adv*. 2019;9:268-277. https://doi.org/10.1039/c8ra09082c.

30. Lee SJ, Park SA, Heo DN, et al. Preparation of electrospun fibrous scaffold containing silver sulfadiazine for biomedical applications. *J Nanosci Nanotechnol*. 2016;16:8554-8558. https://doi.org/10.1166/jnn.2016.12481.

31. Ashtikar M, Wacker MG. Nanopharmaceuticals for wound healing— lost in translation? *Adv Drug Deliv Rev*. 2018;129:194-218. https://doi.org/10.1016/j.addr.2018.03.005.

32. Bernardo MP, Coelho LF, de Lima B, Cristian J, et al. Isolation and characterization of bacterial producers of optically pure D(−) and L(+) lactic acid. *African J Microbiol Res*. 2013;7(21):2618-2628. https://doi.org/10.5897/AJMR2013.5388.

33. Immich APS, Arias ML, Carreras N, Boemo RL, Tornero JA. Drug delivery systems using sandwich configurations of electrospun poly(lactic acid) nanofiber membranes and ibuprofen. *Mater Sci Eng C*. 2013;33(7):4002-4008. https://doi.org/10.1016/j.msec.2013.05.034.

34. Gupta B, Revagade N, Hilborn J. Poly(lactic acid) fiber: an overview. *Prog Polym Sci*. 2007;32:455-482. https://doi.org/10.1016/j.progpolymsci.2007.01.005.

35. Chiang MF, Wu TM. Synthesis and characterization of biodegradable poly(L-lactide)/layered double hydroxide nanocomposites. *Compos Sci*. 2010;70(9):110-115. https://doi.org/10.1007/s00289-014-1184-4.

36. Román MSS, Holgado MJ, Salinas B, Rives V. Drug release from layered double hydroxides and from their polylactic acid (PLA) nanocomposites. *Appl Clay Sci*. 2013;71:1-7. https://doi.org/10.1016/j.clay.2012.10.014.

37. Mascarenhas BC, Tavares FA, Paris EC. Functionalized faujasite zeolite immobilized on poly(lactic acid) composite fibers to remove dyes from aqueous media. *J Appl Polym Sci*. 2020;137(15):48561-48573. https://doi.org/10.1002/app.48561.

38. Aw B, Kirby WM, Sherris JC, Turck M. Antibiotic susceptibility testing by a standardized single disk method. *Am J Clin Pathol*. 1966;45(4):493-496.

39. Balcomb B, Singh M, Singh S. Synthesis and characterization of layered double hydroxides and their potential as nonviral gene delivery vehicles. *ChemistryOpen*. 2015;4:137-145. https://doi.org/10.1002/open.201402074.

40. Cavani F, Trifirò F, Vaccari A. Hydrotalcite-type anionic clays: preparation, properties and applications. *Catal Today*. 1991;11(2):173-301. https://doi.org/10.1016/0920-5861(91)80068-K.

41. Venkataraman M, Nagarsenker M. Silver sulfadiazine nanosystems for burn therapy. *AAPS PharmSciTech*. 2013;14(1):254-264. https://doi.org/10.1208/s12249-012-9914-0.

42. Costa FR, Leuteritz A, Wagenknecht U, Jehnichen D, Häußler L, Heinrich G. Intercalation of Mg–Al layered double hydroxide by anionic surfactants: preparation and characterization. *Appl Clay Sci*. 2008;38:153-164. https://doi.org/10.1016/j.clay.2007.03.006.

43. Halajnia A, Oustan S, Naja N, Khataee AR, Lakzian A. Adsorption–desorption characteristics of nitrate, phosphate and sulfate on Mg–Al layered double hydroxide. *Appl Clay Sci*. 2013;81:305-312. https://doi.org/10.1016/j.clay.2013.05.002.

44. Shao W, Wu J, Wang S, Huang M, Liu X, Zhang R. Construction of silver sulfadiazine loaded chitosan composite sponges as potential wound dressings. *Carbohydr Polym*. 2017;157:1963-1970. https://doi.org/10.1016/j.carbpol.2016.11.087.

45. Fajardo AR, Lopes LC, Caleare AO, et al. Silver sulfadiazine loaded chitosan /chondroitin sulfate films for a potential wound dressing application. *Mater Sci Eng C*. 2013;33(2):588-595. https://doi.org/10.1016/j.msec.2012.09.025.

46. Yang K, Yan LG, Yang YM, et al. Adsorptive removal of phosphate by Mg–Al and Zn–Al layered double hydroxides: kinetics, isotherms and mechanisms. *Sep Purif Technol*. 2014;124:36-42. https://doi.org/10.1016/j.seppur.2013.12.042.

47. Chaves L, Bugatti V, Livi S, Gorrasi G. Phosphonium ionic liquid as interfacial agent of layered double hydroxide: application to a pectin matrix. *Carbohydr Polym*. 2018;182(October 2017):142-148. https://doi.org/10.1016/j.carbpol.2017.10.101.

48. Constantino VRL, Pinnavaia TJ. Basic properties of $Mg^{2+}_{1-x}Al^{3+}_x$ layered double hydroxides intercalated by carbonate, hydroxide, chloride, and sulfate anions. *Inorg Chem*. 1995;34(4):883-892. https://doi.org/10.1021/ic00108a020.

49. Bernardo MP, Moreira FKV, Ribeiro C. Synthesis and characterization of eco-friendly Ca-Al-LDH loaded with phosphate for agricultural applications. *Appl Clay Sci*. 2017;137:143-150. https://doi.org/10.1016/j.clay.2016.12.022.

50. Shao W, Liu H, Liu X, et al. Development of silver sulfadiazine loaded bacterial cellulose/sodium alginate composite films with enhanced antibacterial property. *Carbohydr Polym*. 2015;132:351-358. https://doi.org/10.1016/j.carbpol.2015.06.057.

51. Jaśkaniec S, Hobbs C, Seral-ascaso A, Co J. Low-temperature synthesis and investigation into the formation mechanism of high quality Ni–Fe layered double hydroxides hexagonal platelets. *Sci Rep*. 2018;8:4-11. https://doi.org/10.1038/s41598-018-22630-0.

52. Agnihotri N, Gupta V, Joshi RM. Aerobic bacterial isolates from burn wound infections and their antibiograms—A five-year study. *Burns*. 2004;30:241-243. https://doi.org/10.1016/j.burns.2003.11.010.

53. Russell AD, Hugo WB. Antimicrobial Activity and Action of Silver. Ellis GP, Luscombe DK, eds *Prog Med Chem* 1994;31:351–366.

54. Strydom SJ, Rose WE, Otto DP, Liebenberg W, De VMM. Poly (amidoamine) dendrimer-mediated synthesis and stabilization of silver sulfonamide nanoparticles with increased antibacterial activity. *Nanomedicine Nanotechnology, Biol Med*. 2013;9(1):85-93. https://doi.org/10.1016/j.nano.2012.03.006.

55. Souza ME De, Verdi CM, Andrade ENC De, Santos RC V. Antiviral and Antimicrobial (Antibacterial) Potentiality of Nano Drugs. Elsevier Inc.; 2019. https://doi.org/10.1016/B978-0-12-814029-1.00012-0.

56. Mishra G, Dash B, Pandey S. Layered double hydroxides: a brief review from fundamentals to application as evolving biomaterials. *Appl Clay Sci*. 2018;153(October 2017):172-186. https://doi.org/10.1016/j.clay.2017.12.021.

57. Chen H, Lin J, Zhang N, Chen L, Zhong S, Wang Y. Preparation of MgAl-EDTA-LDH based electrospun nanofiber membrane and its adsorption properties of copper(II) from wastewater. *J Hazard Mater*. 2017;345:1-9. https://doi.org/10.1016/j.jhazmat.2017.11.002.

58. Bi X, Zhang H, Dou L. Layered double hydroxide-based nanocarriers for drug delivery. *Pharmaceutics*. 2014;6:298-332. https://doi.org/10.3390/pharmaceutics6020298.

59. Romeo V, Gorrasi G, Vittoria V. Encapsulation and exfoliation of inorganic lamellar fillers into polycaprolactone by electrospinning. *Biomacromolecules*. 2007;8:3147-3152.

60. Andre RS, Pavinatto A, Mercante LA, Paris EC, Mattoso LHC, Correa DS. Improving the electrochemical properties of polyamide 6/polyaniline electrospun nanofibers by surface modification with

ZnO nanoparticles. *RSC Adv.* 2015;5(90):73875-73881. https://doi.org/10.1039/c5ra15588f.

61. Oliveira JE, Mattoso LHC, Orts WJ, Medeiros ES. Structural and morphological characterization of micro and nanofibers produced by electrospinning and solution blow spinning: a comparative study. *Adv Mater Sci Eng*. 2013;2013:1-14.

62. Bernardo MP, Guimarães GGF, Majaron VF, Ribeiro C. Controlled release of phosphate from layered double hydroxide structures: dynamics in soil and application as smart fertilizer. *ACS Sustain Chem Eng.* 2018; 6(4):5152-5161. https://doi.org/10.1021/acssuschemeng.7b04806.

63. Munteanu B, Dumitriu R, Profire L, et al. Hybrid nanostructures containing sulfadiazine modified chitosan as antimicrobial drug carriers. *Nanomaterials.* 2016;6(11):207. https://doi.org/10.3390/nano6110207.

64. Sobhanian P, Khorram M, Hashemi S, Mohammadi A. Development of nanofibrous collagen-grafted poly(vinyl alcohol)/gelatin/alginate scaffolds as potential skin substitute. *Int J Biol Macromol.* 2019: #pagerange#. https://doi.org/10.1016/j.ijbiomac.2019.03.045.

65. Liu X, Gan H, Hu C, et al. Silver sulfadiazine nanosuspension-loaded thermosensitive hydrogel as a topical antibacterial agent. *Int J Nanomedicine.* 2019;289-300.

SUPPORTING INFORMATION

Additional supporting information may be found online in the Supporting Information section at the end of this article.